Available online at www.sciencedirect.com
SCIENCE DIRECT
Thermochimica Acta 437 (2005) 87–99
thermochimica acta
www.elsevier.com/locate/tca

Comparison of the kinetics of thermal decomposition of biological substances between thermogravimetry and a fielded pyrolysis bioaerosol detector

A. Peter Snyder [a,*], Waleed M. Maswadeh [a], Charles H. Wick [a], Jacek P. Dworzanski [b], Ashish Tripathi [b]

[a] *Edgewood Chemical Biological Center, Research and Technology Directorate, Building E3160, Aberdeen Proving Ground, MD 21010-5424, USA*
[b] *Geo-Centers, Inc., Building E3160, Aberdeen Proving Ground, MD 21010-5424, USA*

Received 30 December 2004; received in revised form 5 May 2005; accepted 8 June 2005
Available online 20 July 2005

Abstract

Thermal decomposition processes were investigated for Bacillus Gram-positive spores. Thermogravimetry analysis (TGA) experiments at 200 K min^{-1} produced a temporal evolution of biochemicals from the spores. Qualitative and quantitative aspects such as peak resolution, peak ratios, peak positions, and temperature maxima are compared and contrasted in the thermal weight loss and differential thermogravimetry (DTG) curves for different Bacillus bacterial spores. The TGA experimental data were used to generate the activation energy and frequency factor Arrhenius equation parameters. These parameters were used to produce TGA and the negative of the first derivative of the TGA (−DTG) decomposition model curves, and the latter are compared to their respective bacterial experimental TGA and −DTG profiles for validation and modeling purposes. The thermal decomposition model is also shown to have application in the prediction of weight loss profiles at significantly higher heating rates than that from the laboratory TGA system. The model thermal decomposition profiles are applied in comparisons to the total ion chromatograms of *Bacillus atrophaeus* bacterial spores generated by an outdoors fielded pyrolysis–gas chromatography–ion mobility spectrometry (Py–GC–IMS) bioaerosol detection system. Pyrolysis at a high heating rate of 3300 K min^{-1} was used. The bioaerosol detection system provides very similar qualitative information to the TGA and −DTG experimental and model profiles.

Keywords: Thermogravimetry; TGA; Pyrolysis; Gas chromatography; Ion mobility spectrometry; Bacillus spores; Thermal weight loss; Kinetics; Rate of reaction; Arrhenius equation; Bacteria

1. Introduction

Thermal decomposition processes have characterized and described the fundamental structures and thermodynamic behavior of many types of compounds including technical organic polymer, pharmaceutical, composite, and energy producing substances. Controlled thermal processing of substances can yield important information on the heterogeneity, constitution, structural elements, durability, thermodynamics, metastable or polymorphic states of a compound, physical application, and limitations of a compound [1–3]. Differential scanning calorimetry (DSC), microcalorimetry, differential thermal analysis, thermogravimetry analysis (TGA), Curie point, glass and metal tube, and foil are common thermal processing methods and devices for biological substances. Thermal product formation includes light gases, char/tar, inorganic salt deposits, and polar and non-polar organic vapor products. It is the latter that provides the most useful structural and physical parameter information for sample characterization.

Fundamental objectives of thermal processing techniques are the modeling of the rate of sample decomposition, derivation of kinetic parameter constants, and the weight loss information from thermal products. The experimental, sigmoid-shaped, thermal weight loss curve (TGA curve) represents

* Corresponding author. Tel.: +1 410 436 2416; fax: +1 410 436 1912.
E-mail address: apsnyder@apgea.army.mil (A.P. Snyder).

0040-6031/$ – see front matter © 2005 Published by Elsevier B.V.
doi:10.1016/j.tca.2005.06.022

the entire vapor flux of a solid sample with a given set of heating parameters [4–8].

The Arrhenius equation parameters and the rate of reaction equation combined with known time–temperature profiles serve as fundamental mathematical tools and methods to produce visual descriptions and parametric descriptors for the rate of a thermal decomposition reaction. Temperature and the remaining amount of sample during product formation are the variables in model descriptions of the experimental thermal decomposition reactions. A thermal decomposition model provides calculated representations of the experimental TGA curve and the negative of the first derivative of the TGA curve (−DTG curve or −DTG profile). Specific information that can be obtained includes the relevancy of proposed thermal decomposition mechanisms, effect of temperature on a solid sample, rates of product formation, order of the reactions, and Arrhenius equation constants.

Analytes that have been investigated by thermal processes include biochemical and bacterial substances [9–11]. Detection, identification, and characterization of the origin of individual biochemical thermal species in bacteria provide substantial interest in the use of heating methods on biological substances.

DSC is a thermal technique that is used to monitor the inactivation and thermally induced death of microorganisms [12–16]. Different organisms have different thermal tolerances, and the absorption of energy by bacterial components [12,14,17,18] is directly monitored by calorimetry techniques. These changes are generally used to pinpoint and postulate what part(s) of the microbe are irreversibly altered that significantly contribute to the death of the organism [12–15,17,18]. Individual proteins, compounds, and organelles are thermally treated and act as standards to correlate temperature and magnitude of thermal absorption with that of the whole organism calorimetry thermal chromatogram [12–14,17,18]. Thermal changes and thermodynamics are used to characterize microorganism viability. Another key application of DSC and microcalorimetry is in the investigation of the melting and crystallization properties of compounds including pharmaceuticals and proteins [2,3,19].

A limited number of thermal studies have been performed on bacteria and their inherent macromolecules and biochemicals with respect to experimental and model thermal decomposition profiles [16,20]. TGA and −DTG profiles of standard proteins, dipicolinic acid, peptidoglycan, and polyhydroxybutyric acid and their TGA mass spectra were compared to that of the equivalent information from bacteria for biochemical identification purposes [21].

Investigations herein expand on the TGA-mass spectrometry (MS) studies of bacteria where the microbiological percent weight of select biochemicals and biopolymers in bacteria were compared to that of individual thermal events observed in the −DTG profiles of Gram-positive spores and vegetative cells [21]. The current work investigates the modeling potential of the Arrhenius and rate of reaction equations with respect to TGA and −DTG profiles from a laboratory TGA to an outdoors fielded pyrolysis–gas chromatography–ion mobility spectrometry (Py–GC–IMS) bioaerosol detection system for Gram-positive Bacillus spores. The Py–GC–IMS system admits aerosol or liquid suspensions of biological substances onto a quartz frit in a glass tube where pyrolysis takes place [22,23]. The resulting vapor is separated by a GC column and detected by an ion mobility spectrometer. Neutral GC eluate passes through a nickel-63 radioactive ionization source and becomes ionized by proton transfer from proton hydrate gaseous reagent ions. The ions are gated and enter an electrical gradient in an atmospheric pressure drift tube. A Faraday plate detects the ions [24].

The Arrhenius and rate of reaction equations and parameters are shown to satisfactorily model and describe bacterial TGA and −DTG profiles of laboratory experiments as well as thermal data from a fielded Py–GC–IMS bioaerosol detection system. TGA-MS was used as a laboratory adjunct for the investigations of microorganisms in order to characterize and interpret the heating parameter effects and their interrelationships with respect to the outdoor-fielded Py–GC–IMS bioaerosol detector. The TGA-MS was also used to modify, optimize, and refine the heating parameter settings on the pyrolysis module in the Py–GC–IMS.

2. Experimental

2.1. Materials

Proteins in powdered form were purchased from Sigma–Aldrich as follows: insulin (I5500, molecular weight (MW) = 5733), myoglobin (M 0630, MW = 17,200), bovine milk beta-lactoglobulin B (L 8005, MW = 18,276), bovine erythrocyte carbonic anhydrase (C 3934, MW = 29,024), ovalbumin (A 2512, MW = 44,300), and bovine serum albumin (BSA, A 7638, MW = 66,430). The proteins were applied onto the sample pan in milligram quantities in the dry powder form.

2.2. Bacteria preparation procedures

Gram-positive spores of *Bacillus cereus* ATCC 6464, *Bacillus atrophaeus* (formerly *Bacillus subtilis* var. *globigii*) [25], and *Bacillus megaterium* were prepared as described in the following procedures. A Bacillus culture was streaked for isolation onto an agar plate containing trypticase soy agar and 5% sheep's blood and incubated overnight at 37 °C. A single colony was streaked onto an agar plate and incubated at 37°C for about 4–6 h or until there was visible growth on the plate. The bacterial growth was scraped from the agar plate and was suspended in sterile broth or saline. Five hundred microliters of the bacterial suspension was pipetted onto the surface of nutrient sporulation media in an agar plate and spread evenly with a cell spreader. These plates were incubated at 37 °C for 3 days until spore production

reached 95–98%, and the spore generation was monitored using phase contrast microscopy. Vegetative cells appeared as dark oblong cells in short or long chains except for *B. atrophaeus*. *B. atrophaeus* spores appeared as smaller, highly refractile bodies either within vegetative cells or free-floating. Bacterial growth was scraped from the agar plates, washed twice with 200 mL sterile water, and resuspended in sterile water. All cultures were autoclaved for 20 min to kill both vegetative cells and spores. The killed bacteria were then lyophilized. Organisms used in this study can be and were handled and processed under minimal Biosafety level BSL-1 conditions.

2.3. Instrumentation

2.3.1. TGA-MS system

A Perkin Elmer Pyris 1 TGA was used for biological substance analysis, and a schematic of the TGA-MS system can be found elsewhere [21]. A platinum sample pan (Perkin Elmer part # 319-0263) was freely suspended from the hang-down balance. A sample was deposited as a dry powder onto the platinum sample pan. The TGA furnace assembly was continuously flushed from the top to the bottom of the furnace with helium at 50 mL min^{-1}. The Pyris 1 TGA was used to ramp a sample at 1, 5, 10, 20, 50, 100, and 200 K min^{-1} and was calibrated to a temperature of 870 K. The TGA system was set at an acquisition rate of five temperature weight loss points per second. A heated transfer line was used to continuously transfer the thermally generated vapors to the mass spectrometer system. The 1 m long 180 μm i.d. deactivated fused silica transfer line (Alltech, # 602010) was heated and maintained at a constant temperature of 220 °C. A Perkin Elmer TurboMass Gold mass spectrometer was used as the detector, and isobutane was the chemical ionization (CI) reagent gas. The CI mode was tuned by adjusting the flow rate of isobutane such that the intensity ratio of ions *m*/*z* 57–43 was maintained at a 2:1 ratio according to the recommendations of the manufacturer. The pressure inside the mass spectrometer at which this ratio was reached and maintained was 4 × 10E-4 Torr. The mass spectrometer is capable of acquiring scans at a maximum rate of 6000 Da s^{-1}, and it was used to scan masses from 60 to 560 Da with a 1 Da mass resolution. This procedure allowed the MS system to acquire up to five mass spectra per second, and this data acquisition speed matched that of the TGA. The TGA calibration was performed using the manufacturer recommended magnetic transition temperature approach with different standards. Alumel (magnetic transition temperature = 427.36 K), nickel (magnetic transition temperature = 628.46 K), and perkalloy (magnetic transition temperature = 869.16 K) magnetic substances were deposited on the platinum pan [26]. The pan was heated from 25 to 1000 K at 20 K min^{-1}. When the metals reached their respective magnetic transition temperature, they lost their magnetic field and registered a rapid weight loss against the pull of an external magnet. The temperature at which each magnetic transition occurred was calibrated to the magnetic transition temperature of the respective metal standard.

2.3.2. Py–GC–IMS system

The pyrolysis sample processor in the Py–GC–IMS consisted of a Pyrex tube (4 mm i.d., 8 mm o.d., and 5 cm length) with a quartz microfiber filter (type QM-A, thickness 0.45 mm, from Whatman, Hillsboro, OR) supported by a Pyrex frit inside the tube [22,23]. The Pyrex tube was wrapped with a resistive heater filament (Omega Engineering, Stamford, CT). The heating apparatus was used in two modes of operation: (a) a 10 s mode with the maximum temperature in the tube at 120 °C for drying the moisture and other low boiling volatiles after a sample was deposited on the filter and (b) a subsequent pyrolysis mode with a maximum temperature of 460 °C in 7 s [22,23,27].

Samples were deposited as water suspensions on the quartz microfiber filter. The resulting pyrolysis products were transferred through a Silcosteel™ tube (Quadrex, New Haven, CT, USA) at an isothermal temperature of 200 °C. The injection valve transferred a portion of the sample into the GC column (stainless steel, 4 m × 0.50 mm i.d. Ultra Alloy) coated with a 0.10 μm layer of poly(dimethylsiloxane) from Quadrex (New Haven, CT, USA). The GC was kept in an isothermal mode at 40 °C prior to pyrolysis. Ten seconds after the pyrolysis event, the GC was ramped from 40 to 140 °C at 120 °C min^{-1}. The airflow through the IMS detector was 15 mL min^{-1}. The temperatures of the pyrolyzer, three-way injection valve, and GC column were monitored by using type K thermocouples connected to in-house constructed control electronic boards interfaced to a laptop computer.

The pyrolyzer was kept at atmospheric pressure with a flow of atmospheric room air, and the pyrolyzate was transferred into the GC column during pyrolysis using a three-way valve. The exit of the temperature programmable GC column was inserted behind the ring shaped nickel-63 ring ion source of the Chemical Agent Monitor IMS detector (General Dynamics, DeLand, FL). The sub-ambient pressure generated by the IMS pump at the GC column outlet was utilized as a driving force for the air carrier gas flow during the pyrolyzate transfer and injection steps into and through the GC column. Further details of the Py–GC–IMS system configuration and parameters can be found elsewhere [23].

2.4. Prediction model theory for biological substance thermal decomposition

The pyrolysis temperature gradient in the Py–GC–IMS bioaerosol detection system heats a biological sample at a rate of 3300 K min^{-1}, and this was measured by a type K thermocouple. Thirty three hundred per Kelvin per minute is significantly faster than the maximum rate (200 K min^{-1}) of the laboratory TGA system. Thus, a predictive or modeling approach for the experimental TGA thermal information was formulated in order to evaluate rapid heating decomposition processes occurring from a biological sample in the pyrolysis

source of the bioaerosol detector. Modeling of the biological TGA curve also can provide information toward the understanding of the experimental thermal behavior of small biochemical species, biopolymers, and bacteria. In order to simplify the modeling procedure for a TGA curve, a number of assumptions must be made.

Assumption 1. Since the bacterial analyte is composed of many biological components and substances, it is assumed that there are no biochemical interactions between the major classes of biochemicals and biopolymers during the thermal decomposition process. The assumption is that, for example, the thermal degradation reactions of the protein component do not influence or interact with that of the carbohydrate, DNA, RNA, peptidoglycan, etc., components of the bacterium. This allows for extraction of pseudo-Arrhenius equation kinetics parameter information.

Assumption 2. The thermal degradation reactions of the major classes of biochemicals and biopolymers proceed in parallel and not in series. That is and, for example, the set of thermal reactions governing the decomposition of proteins are independent in time and sequence with respect to the set of thermal degradation reactions for the carbohydrate, DNA, RNA, etc., components. The biological decomposition processes between each major class of biochemical and biopolymer are viewed as independent, and non-interactive.

Assumption 3. Each of the local maxima in an experimental −DTG curve (e.g. Fig. 1a) is a direct result of one or more independent parallel reaction pathways as described in Assumption 2.

Assumption 4. The parallel thermal decomposition reactions that describe each major class of biochemical and biopolymer in a bacterium proceed under first order kinetics.

Based on these four assumptions, a mathematical model for the thermal decomposition kinetics of biological samples can be proposed. The model is based on the linear summation of the independent thermal decomposition reaction pathways of individual biochemical components in complex analytes such as bacteria.

Step 1. Assumption 1 allows the thermally decomposing biological sample to be viewed as an agglomerate of multiple biochemicals and biopolymers decomposing simultaneously. Thus, the biological sample can be characterized as:

$$W = \sum w_i, \quad i = 1, \ldots, p \tag{1}$$

W is the total weight of the sample at time t and w_i is that part of sample weight W that follows parallel reaction pathway i at time t. There are p numbers of parallel reaction pathways proceeding concurrently.

Step 2. Assumption 2 describes the rate of sample weight loss as an aggregate of the rate of weight loss from each of the parallel reaction pathways. The first derivative of Eq. (1) with respect to time produces the rate of weight loss:

$$\frac{dW}{dt} = \frac{\sum dw_i}{dt}, \quad i = 1, \ldots, p \tag{2}$$

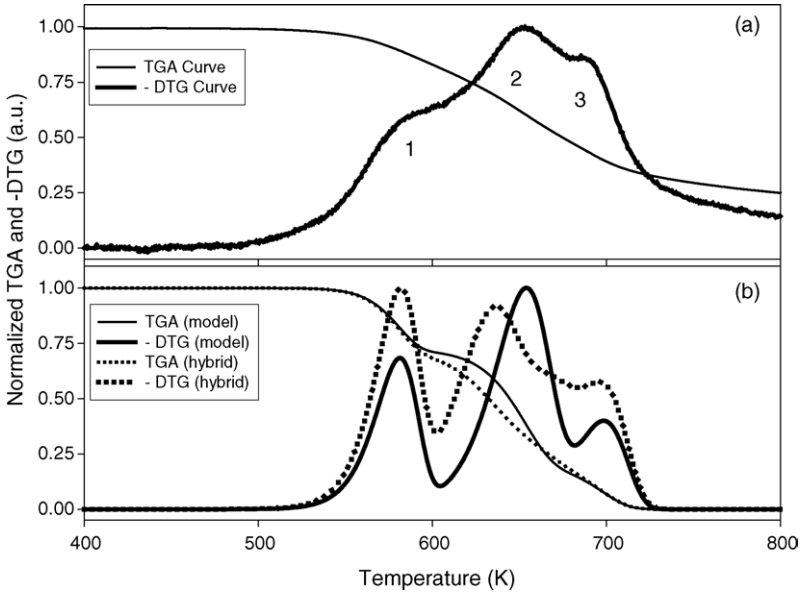

Fig. 1. (a) Sigmoid-shaped, normalized experimental TGA curve, and the negative of the first derivative of the TGA curve (−DTG, bold curve) of *B. atrophaeus* spores from the TGA at a heating rate of 200 K min^{-1}. (b) Thin solid curve, model TGA; bold solid curve, model −DTG; thin dotted curve, hybrid TGA; bold dotted curve, hybrid −DTG. Both TGA curves derive from the Arrhenius equation constants for the *B. atrophaeus* first and third thermal events. The second event consists of a composite of the Arrhenius equation constants from the average TGA curves of six model proteins (see Section 2). Thermal events are labeled 1–3.

Step 3. Assumption 4 relates the use of first order decomposition kinetics for each of the p reaction pathways. Thus, the following first order expression is used:

$$\frac{dW}{dt} = -\sum w_{i0} A_i \exp\left(\frac{-E_i}{RT}\right)(1 - x_i), \quad i = 1, \ldots, p \tag{3}$$

A_i is the frequency factor, E_i the activation energy, R the ideal gas constant, T the temperature at time t, w_{i0} the initial weight of that part of the sample that follows parallel reaction pathway i, and x_i is the conversion of a biochemical component that follows parallel reaction pathway i at time t.

Step 4. To solve Eq. (3), A_i and E_i must be determined. From Assumption 3, the number of local maxima in a −DTG profile of a biological substance determines the number of reaction pathways where p is the number of times the expression $d(dW/dt)/dT = 0$ is true. This expression occurs at a thermal maximum characterized by a T_{max} temperature in the −DTG curve. Using the condition for a temperature maximum in conjunction with Eq. (3), the following equation is obtained as reported by Braun and Burnham [5].

$$\ln\left(\frac{H_r}{T_{max,i}^2}\right) = \frac{-E_i}{RT_{max,i}} + \ln\left(\frac{A_i R}{E_i}\right) \tag{4}$$

H_r is the linear heating rate and $T_{max,i}$ is the temperature at which the rate of decomposition due to pathway i is at a maximum. Eq. (3) shows that the A_i frequency factor is a constant. Braun and Burnham [5], however, use a distributed activation energy (DAE) where A_i is a function of E_i and the full width at half height (FWHH) of a thermal peak in a −DTG curve. A −DTG curve of a bacterial thermal degradation experiment yields highly convoluted, poorly resolved peaks (vide infra). Calculation of the FWHH parameter would yield misleading results because of the poor resolution between peaks. Therefore, the conventional rate of reaction, Eq. (3), is employed. Eq. (4) characterizes E_i and A_i. By performing multiple TGA experiments at different heating rates, the $T_{max,i}$ values are obtained for each heating rate. A plot of $\ln(H_r/T_{max,i}^2)$ and $1/T_{max,i}$ produces a straight line if Assumption 1 is valid. The slope of the straight line is $-E_i/R$, and the intercept is $\ln(A_i R/E_i)$. From the slope and the intercept value of the straight line, the value of E_i and A_i are determined.

Using the values for A_i, E_i and the time–temperature history of the pyrolysis heating profile, Eq. (3) is solved by the finite element method or Δ(time) with the initial condition that at time $t = 0$, $x = 0$.

3. Results and discussion

3.1. TGA linear programmed heating characteristics of *B. atrophaeus*

Fig. 1a presents the sigmoid-shaped, experimental TGA, and −DTG curves for *B. atrophaeus*. The heating rate applied to the solid sample was 200 K min^{-1}, which is the maximum heating rate of the TGA system. Three distinct thermal events can be observed, and they are labeled 1–3. Previous TGA-MS studies of *B. atrophaeus* spores showed that event 1 has mass spectral characteristics of picolinic acid and cell wall peptidoglycan [21]. For the investigation of the rate of weight loss, *B. atrophaeus* samples were subjected to decomposition at various heating rates from 2 to 200 °C min^{-1}, and Fig. 2 shows that the overall shapes and appearance of the −DTG profiles are similar. The three thermal events or peaks in Fig. 1a are

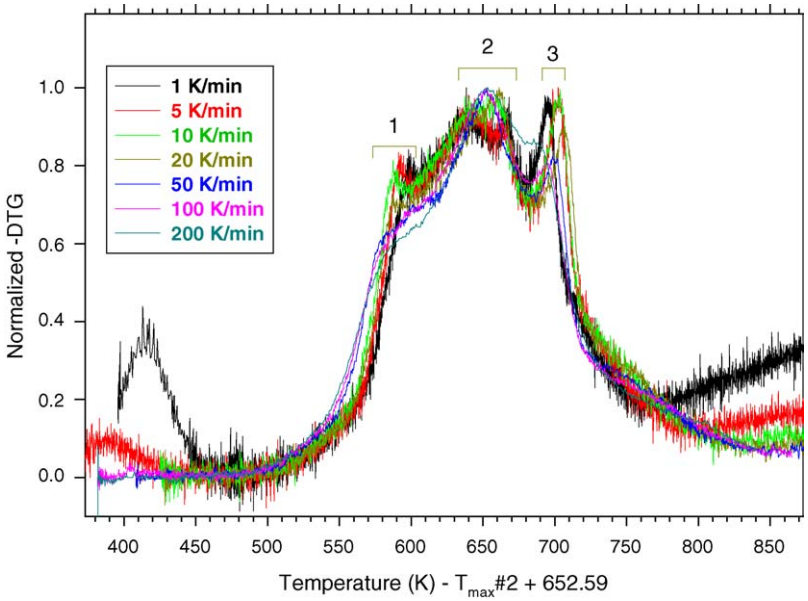

Fig. 2. Temperature vs. −DTG profiles of *B. atrophaeus* at heating rates of 1, 5, 10, 20, 50, 100, and 200 K min^{-1}.

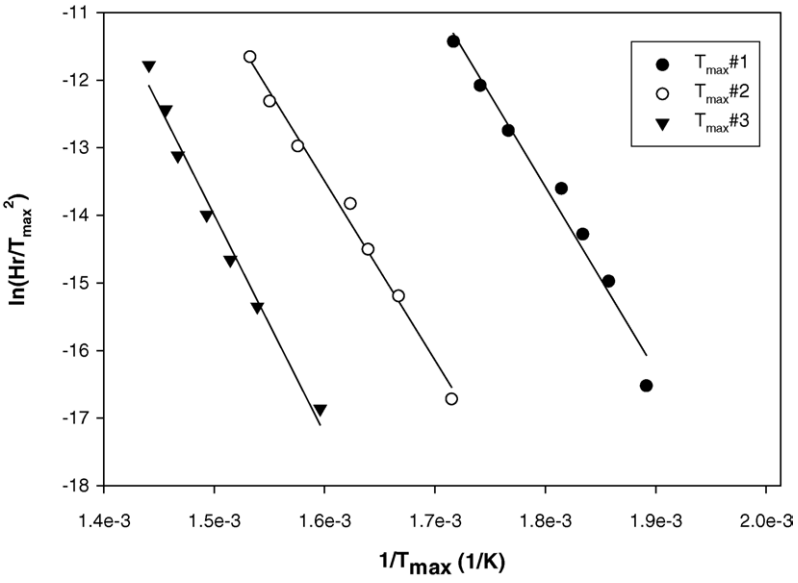

Fig. 3. Linear Arrhenius equation plots of the three thermal events from the experimental −DTG curve for *B. atrophaeus* in Fig. 1a.

transformed into Arrhenius plots (Fig. 3) according to Eq. (4) in Section 2.4, where H_r is the heating rate at 200 K min^{-1}, R the 1.987 cal (g mol K)$^{-1}$, and T_{max} is the temperature at the maximum of a thermal decomposition event. The slope $-E/R$ and y-intercept $\ln(AR/E)$ provide the activation energy, E in kcal/mol, and the effective collision frequency factor, A, respectively, for each thermal event. Table 1 provides the E and A constants for each thermal event in the experimental −DTG curves of *B. atrophaeus*. The regression coefficients, r^2, for the three plots in Fig. 3 have excellent linearity characteristics at better than 0.97, and this supports the first order kinetics hypothesis in Assumption 4. Eq. (3) allows a model TGA curve (Fig. 1b, thin solid curve) to be constructed and compared directly to the experimental TGA curve (Fig. 1a). The weight loss rate can be calculated for a given time–temperature point on a thermal decomposition profile. Fig. 1b presents the model −DTG (bold solid) profile for *B. atrophaeus*. A comparison of the experimental (Fig. 1a) and model (Fig. 1b) TGA curves shows a high degree of correlation over the temperature range. However, the model displays a noticeable variation from linearity in the weight loss region between 600 and 700 K. This produces a better resolution of the model −DTG curve (Fig. 1a, bold solid) compared to the experimental −DTG curve (Fig. 1a). Note that the model −DTG curve displays the three thermal events at approximately the same T_{max} values as that of the experimental −DTG curve (Fig. 1a). However, event 3 is shifted from 694 K in the experimental −DTG curve to 698 K (0.6%

Table 1
Arrhenius linear equation parameters for proteins and bacterial components

Name	Thermal event	Activation energy, E (kcal/mol)	Frequency factor, A	r^2	Comments
B. atrophaeus spores	1	54.06	5.71E19	0.978	a
	2	52.64	8.36E16	0.991	b
	3	64.21	2.72E19	0.984	c
Insulin	2	51.18	1.05E17	0.995	5.7 kDa
Myoglobin	2	41.68	1.32E13	0.999	16.9 kDa
Beta-lactoglobulin	2	40.66	3.95E12	0.997	18.4 kDa
Carbonic anhydrase	2	41.83	1.58E13	0.997	29.1 kDa
Ovalbumin	2	45.30	1.34E15	0.996	42.7 kDa
BSA	2	43.24	1.66E14	0.999	64 kDa
B. cereus spores	1	41.13	1.65E14	0.990	d
	2	37.28	2.74E11	0.999	b
	3	65.10	5.00E19	0.977	c
B. megaterium spores	1	50.21	4.24E17	0.993	d
	2	39.79	3.65E12	0.997	b
	3	65.72	1.08E20	0.996	c

a, Thermal event 1 contains mass spectral features of DPA and peptidoglycan [21]; b, thermal event 2 contains mass spectral features of protein and peptidoglycan [21]; c, fragments of fatty acids (data not shown); d, thermal event 1 contains mass spectral features of DPA, PHBA, and peptidoglycan [21].

difference) in the model −DTG curve. The model −DTG curve provides an approximation for the three thermal events compared to the experimental −DTG curve. This was a first attempt at modeling a rate of reaction thermal weight loss profile from a bacterium. The model −DTG curve cannot provide mass spectral information, however, this was satisfactorily supplied by the total ion mass chromatogram data [21].

The second thermal event was shown to consist mainly of protein species by the mass spectral information [21]. Since a bacterium contains approximately 50% protein by weight and is the predominant biochemical component, this information was used to replace the second event in the *B. atrophaeus* model −DTG curve in Fig. 1b. A hybrid −DTG curve was constructed where the first and third events were retained from the experimental −DTG curve of *B. atrophaeus,* and the second event was replaced with a composite of six proteins (Table 1). The experimental −DTG curves of the proteins are presented elsewhere [21], and their Arrhenius equation plots are presented in Fig. 4. They all display a high degree of linearity (Table 1), and the sigmoid-shaped experimental TGA curve of each protein (data not shown) was used to generate the Arrhenius equation constants. All six protein TGA profiles were combined such that each contributed one-sixth of the total protein information. The chosen proteins span a mass range of 5700–66,400 Da. This adequately covers the mass range of proteins contained in *B. atrophaeus* [28,29]. The selected proteins provide a representative sampling of the bacterial proteins' mass range.

Fig. 1b presents the hybrid TGA curve (light dotted curve) and the hybrid −DTG profile (bold dotted curve), and they can be directly compared to the experimental (Fig. 1a) and model (Fig. 1b) TGA and −DTG curves, respectively. The dominant second thermal event in the hybrid −DTG curve (bold dotted curve) is broader than that of the model −DTG (bold solid curve) in Fig. 1b. The second thermal event in the hybrid −DTG curve encompasses an area in a more similar fashion to the experimental −DTG curve (Fig. 1a) than that of the model −DTG curve (Fig. 1b). The T_{max} of the first event is the same in the experimental model and hybrid −DTG profiles. The T_{max} of the second event in the hybrid −DTG curve (bold dotted curve) is shifted from the experimental −DTG curve value of 652 K (Fig. 1a) to a lower temperature value of 636 K. The third T_{max} of 697 K in the −DTG model and hybrid curves is slightly higher than that of the experimental −DTG curve T_{max} at 694 K. The hybrid −DTG curve appears to provide an advantage over the model curve in quantitative modeling aspects compared to the experimental −DTG curve. The model −DTG curve provides a competitive edge in the qualitative T_{max} aspect of the thermal events compared to the experimental −DTG curve.

3.2. Other Bacillus TGA linear programmed heating profiles

Fig. 5a presents 200 K min^{-1} thermal weight loss information for *B. cereus*, and the sigmoid-shaped experimental TGA curve is similar to that of *B. atrophaeus* in Fig. 1a. The experimental −DTG curve (bold solid curve) shows two clear thermal events, and a third thermal peak appears as a slight shoulder on the high temperature side of the second peak. The Arrhenius parameters used in the modeling of the experimental TGA curve are listed in Table 1. For *B. cereus*, it appears that the model −DTG curve (dashed curve) is more similar to the experimental −DTG curve with respect to resolution and quantitation than that of *B. atrophaeus* in Fig. 1. The third peak is not apparent in the model −DTG curve. The hybrid protein −DTG curve (dotted curve) in Fig. 5a provides a satisfactory representation of the first thermal peak,

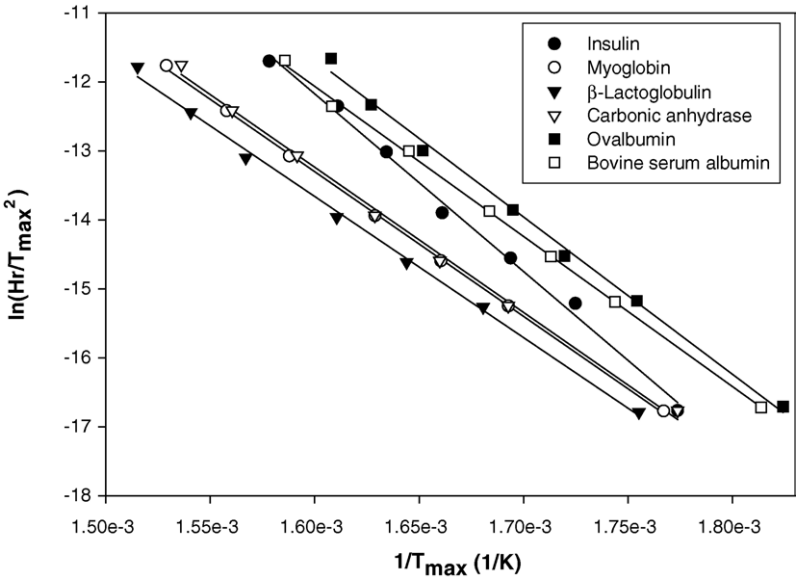

Fig. 4. Linear Arrhenius equation plots from the single peak, experimental −DTG curves [21] from each of the six model proteins.

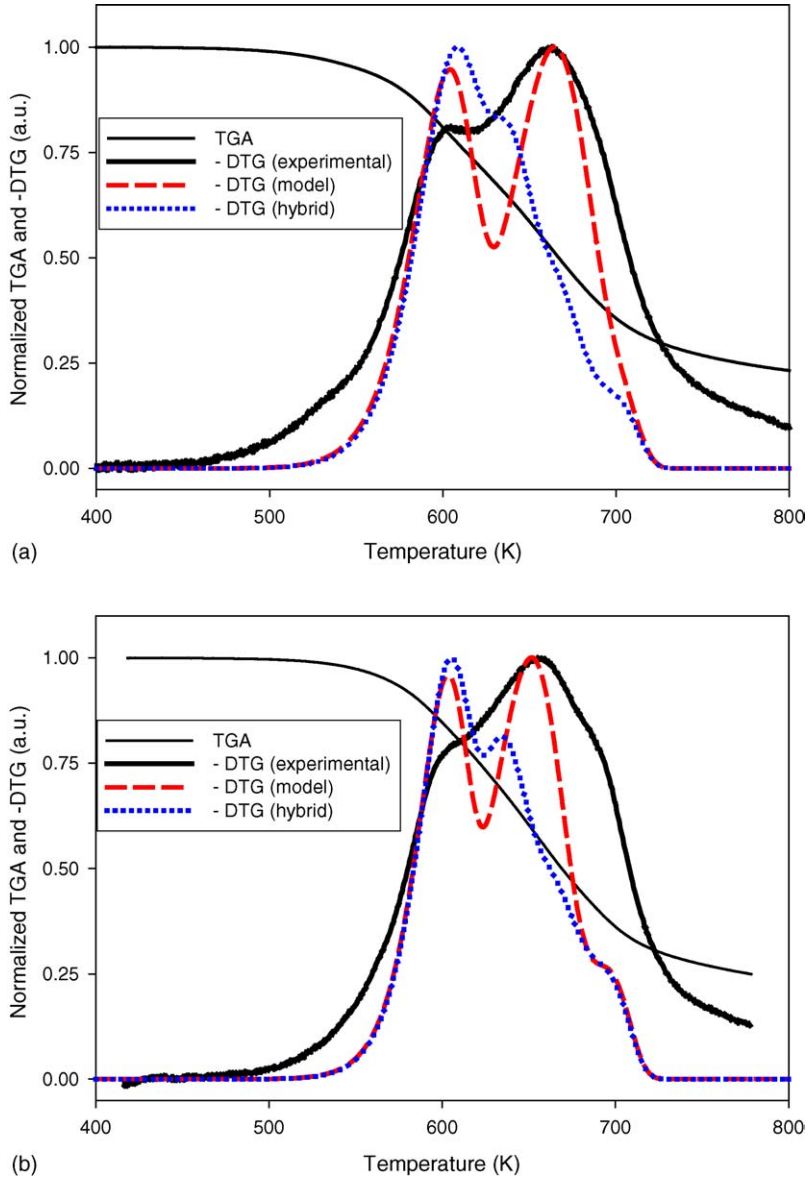

Fig. 5. Sigmoid-shaped experimental TGA (thin solid line) and experimental, (bold solid profile), model (dashed) and hybrid (dotted) −DTG profiles of (a) *B. cereus* spores and (b) *B. megaterium* spores at 200 K min^{-1}.

but it displays a poorer representation of the second peak. The hybrid −DTG curve provides a low intensity yet distinct third thermal peak that matches the T_{max} of the experimental −DTG curve. The second peak of the hybrid -TG curve (dotted curve) is shifted to a lower temperature (637 K) than that of the experimental (662 K) and model (665 K) −DTG curves, and this shift is similar in magnitude and direction to the hybrid −DTG curve of *B. atrophaeus* in Fig. 1b. The model −DTG curve is similar to the experimental −DTG curve (Fig. 5a).

Fig. 5b presents experimental TGA curve and −DTG model information for the thermal processing of *B. megaterium*. Two intense peaks are observed in all three −DTG curves, and a third appears as a shoulder on the high temperature side of peak 2 in all three −DTG curves. The sigmoid-shaped experimental TGA curve is similar in appearance to that of *B. atrophaeus* and *B. cereus*. The Arrhenius parameters used in the modeling of the experimental TGA curve for *B. megaterium* are listed in Table 1. The model −DTG curve (dashed curve) displays a satisfactory T_{max} match for all three thermal peaks with respect to the experimental −DTG curve. The hybrid −DTG curve (dotted curve) provides a satisfactory T_{max} match to peaks 1 and 3 but has a lower T_{max} (635 K) compared to that of the experimental −DTG curve (653 K) for peak 2.

3.3. TGA thermal weight loss comparison of the bacilli

General trends can be observed for the three bacilli in Figs. 1 and 5. The experimental TGA curves for all three

bacilli show that 75% of the sample is vaporized and approximately 25% remains as char/tar on the heating pan. The experimental −DTG envelopes generally reside in the same temperature range, and they display two clear thermal events with the third event as a shoulder on the high temperature side of peak 2. The model −DTG curves generally provide a satisfactory T_{max} match for all three peaks to that of their respective experimental −DTG curves, while the hybrid −DTG curves provide a satisfactory match with peaks 1 and 3. The second peak is dominated by proteinaceous material [21], and an attempt to model that peak with representative proteins in the hybrid −DTG curve appears to be somewhat less than satisfactory for all three bacteria. The hybrid −DTG curve for all three bacteria yield a lower T_{max} for peak 2 compared to that in their respective experimental −DTG curves. All three bacilli (Figs. 1a and 5) show a similar peak amplitude trend for the three peaks in their experimental −DTG curves. *B. cereus* and *B. megaterium* display similar model −DTG curves (dashed curves) where the first and second peaks are of equal magnitude. The third thermal event in the experimental −DTG curve is more noticeable and distinct for *B. atrophaeus* and *B. megaterium* than in *B. cereus*, and this observation for peak 3 is the same in the respective model −DTG curves. An opposite trend is observed in the protein hybrid −DTG curves for the magnitude of peaks 1 and 2 in all three bacteria. They show a hybrid peaks 1–2 ratio that is greater than 1, and for the three experimental –DTG curves (Figs. 1a and 5), the ratio is less than 1.

In these comparisons, it appears that the model −DTG curve provides a relatively better representation of the experimental −DTG curve than that of the hybrid with respect to the T_{max} parameter. However, the hybrid −DTG curve shows a much greater degree of similarity in peak overlap compared to the experimental −DTG curve in all three bacteria than the model −DTG curves. Inclusion of the proteins in the modeling results in a greater degree of peak overlap in the hybrid −DTG curve with respect to the model −DTG curve. Thus, the hybrid case models the experimental −DTG curve to a better degree than the model −DTG curve with respect to the high degree of overlap between peaks 1 and 2.

In general, the model and hybrid −DTG curves provided a good match to the experimental −DTG curve with respect to temperature maxima, but the peak shapes did not match or fit to a satisfactory degree. The model and hybrid plots were not derived from using biochemical component initial fraction weights, w_{i0}, as fitting parameters. Rather, experimental and known values of the initial fraction weights were used in the rate of weight loss (Eq. (3)) for a fit to the experimental −DTG curve. The experimental weight loss values originated between two thermal events or inflection points in the TGA curve. The established known parameters were based on bacterial percent composition values of the major biochemical components and macromolecular biopolymers [21].

3.4. Thermal modeling of the Py–GC–IMS biodetection system with B. atrophaeus

The information content in a GC–IMS dataspace from the briefcase Py–GC–IMS was examined and shown to provide inherent, invariant fundamental biochemical compounds from Gram-positive spores and vegetative cells as well as Gram-negative cells [11]. Placing a Tee in the GC and arranging the IMS and a time-of-flight mass spectrometer in parallel with each other produced this biochemical information. Peptidoglycan macromolecules from Gram-positive cells and lipopolysaccharide (LPS) surface species in Gram-negative bacteria produced information rich pyrolyzate products [11]. Pyrolysis produced 2-pyridinecarboxamide from the peptide linkages between the polysaccharide macromolecules of peptidoglycan in the Gram-positive species and four 2-hydroxymyristic acid derivative compounds and two straight chain fatty acids from the LPS in Gram-negative cells [11].

The Py–GC–IMS uses a 3300 K min^{-1} heating rate to pyrolyze a solid sample. This does not allow for a TGA weight loss profile that spans a timeframe measured in minutes such as those in Figs. 1, 2, and 5. However, the operation of the Py–GC–IMS system provides temporally selected portions of the thermal products after the pyrolysis event to be admitted into the GC column for separation and IMS detection. Replicate experiments with *B. atrophaeus* spores were performed and pyrolyzate was admitted into the GC column at different time delays after the onset of pyrolysis. Fig. 6a presents a series of 10 GC–IMS chromatograms. Each chromatogram is identified by a 0.5-s interval between 2 and 7 s, where 7 s is the total pyrolysis time. For the first, or left-most, chromatogram in Fig. 6a, very little pyrolyzate vapor was injected into the GC column between 2.0 and 2.5 s after the onset of pyrolysis. The vertical dark line in each GC–IMS dataspace represents the protonated water molecule cluster gaseous reagent ions or reactant ion peak (RIP) [24]. The nickel-63 ring beta energy electron emitter ionizes the atmospheric air. A cascade of reactions that include nitrogen creates a plasma of protonated water clusters inside the nickel ring. As neutral sample elutes from the GC column, proton transfers ionize those species with a proton affinity greater than that of water. The ionized sample appears at a longer IMS drift time, and the protonated water becomes a neutral species. A decrease or disappearance of the RIP results from a proton transfer to an analyte molecule. A reduction or absence of analyte from the GC then allows the RIP to reappear.

The two points at the lower left in Fig. 6b on the graph at 2.25 s represent replicate summations of the GC–IMS dataspace at 2.0–2.5 s (Fig. 6a) after the onset of pyrolysis. The two points represent a total of five replicate experiments, and all subsequent sets of experimental points consist of five replicates. The portion of the GC–IMS dataspace in the summation includes all peak intensities between IMS drift times of 5.2–11 ms and GC retention times of 5.0–50 s. The next set of experimental points at 2.75 s represents replicate summations of the GC–IMS dataspace at 2.5–3.0 s after

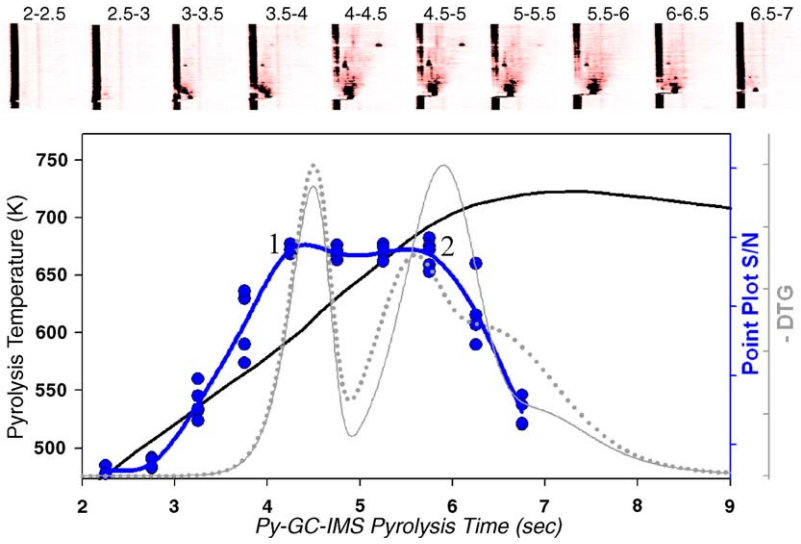

Fig. 6. Py–GC–IMS thermal product information for *B. atrophaeus* spores. (a) Experimental GC–IMS dataspaces that represent successive 0.5 s injections of pyrolyzate vapor products into the GC. (b) The pyrolysis heating temperature is represented by a bold line that reaches a plateau at 7–9 s. A cubic spline profile was constructed about the plotted points (point plot). Each point represents the average of the peak intensity summation in a GC–IMS dataspace from the respective 0.5 s GC injection interval in (a). The gray solid curve represents the −DTG profile of the model TGA curve (not shown), and the dotted curve is the −DTG profile of the hybrid TGA curve (not shown).

pyrolysis. This continues with five replicate experiments per 0.5-s sample introduction period into the GC column. In summary, all Py–GC–IMS experiments utilized a total pyrolysis time of 7 s, and 0.5 s temporal slices of the pyrolyzate vapor was injected into the GC column. Each replicate set of points in Fig. 6b has an example GC–IMS dataspace in Fig. 6a. The GC–IMS dataspace becomes more populated with intensities at 4–6 s pyrolyzate injection times. In most of the GC–IMS dataspaces in Fig. 6a, as GC retention time increases, relatively more biological signals are observed. As the GC retention time increases even further, a lower amount of sample elutes, and the RIP becomes the dominant signal. A cubic spline profile (bold solid curve) was constructed to fit the points in Fig. 6b. The resulting Py–GC–IMS point plot profile clearly shows two thermal events labeled 1 and 2, even though they display a considerable amount of overlap. The pyrolyzer temperature variation (bold line that reaches a plateau at 7–9 s) over the 7 s heating time is shown in Fig. 6b.

Fig. 6b also presents the model and hybrid differential thermal curves of the products from the Py–GC–IMS. The algorithms used for the construction of the model and hybrid −DTG curves in Fig. 1b were also applied to that in Fig. 6b except a rapid heating rate of 3300 K min^{-1} was used instead of a controlled 200 K min^{-1}. Therefore, the model and hybrid differential curves derived from the Py–GC–IMS point plot can be thought of as virtual −DTG 3300 K min^{-1} curves. The T_{max} for peak 1 in the model and hybrid −DTG curves (solid gray and dotted curves, respectively) are the same at 618 K. The peak 2 T_{max} for the hybrid curve is similar to that of the point plot at 680 K (Fig. 6b). Peak 2 for the model curve is somewhat higher in temperature at 693 K. The Py–GC–IMS point plot displays a high degree of peak overlap, and the model and hybrid curves have a very high degree of resolution for the first two thermal peaks. The model and hybrid curves in Fig. 6b display a low intensity peak 3, because the models originate from the TGA three-peak model as used in Fig. 1b. The third peak is absent from the Py–GC–IMS data, and this can be explained by the relatively cold, room temperature IMS detector [11]. It is possible that the biochemical origin of the third peak represents fatty acid species as suggested by mass spectrometry interrogation of the equivalent IMS detector response [11,21]. The fatty acid species pass through the heated GC and are detected by the heated mass spectrometer. However, the parallel IMS system does not register the presence of the fatty acids because of the room temperature characteristic of the detector. Adsorption of the fatty acids onto the cold surfaces of the IMS detector may prevent their detection. Overall, it appears that the Py–GC–IMS system produces a somewhat qualitatively similar experimental −DTG curve compared to that of the model and hybrid curves (Fig. 6b) with respect to the T_{max} values.

3.5. Thermal modeling of the Py–GC–IMS with other bacilli

Fig. 7 presents GC–IMS information and thermal weight loss information from the pyrolysis of *B. cereus* spores with the Py–GC–IMS system. A cubic spline profile (bold solid curve) was constructed to fit the points in Fig. 7b. Model and protein hybrid −DTG curves are superimposed on the experimental GC–IMS point plot (Fig. 7b). Fig. 7a shows successive 0.5 s GC–IMS dataspace spectra of the pyrolysis of *B. cereus*, and Fig. 7b shows replicate points per GC injection time originating from the summation of the GC–IMS dataspace signals. The pyrolysis heating temperature curve

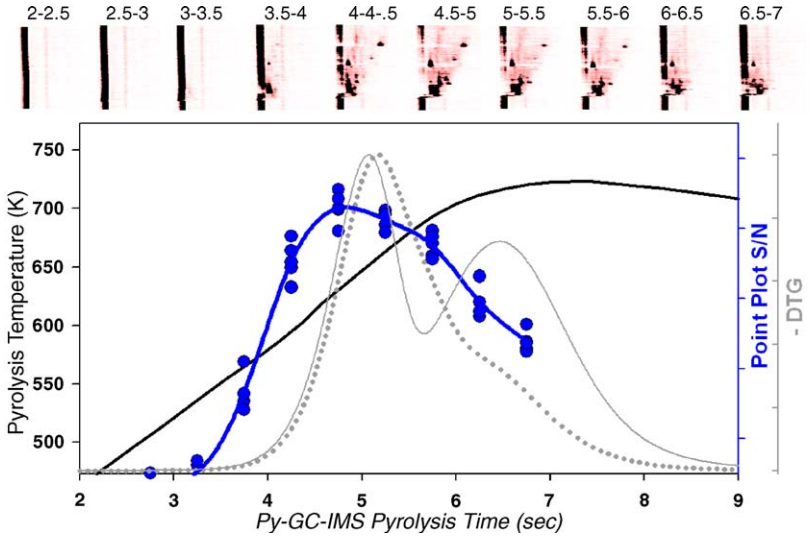

Fig. 7. (a and b) Py–GC–IMS thermal product information for *B. cereus* spores; see Fig. 6 caption for details.

(bold line with a plateau at 7–9 s) is shown in Fig. 7b for the biodetection system. One relatively wide peak is observed in the point plot. Because of the relatively poor resolution, it is possible that a second thermal event is present as a shoulder at 5.75 s on the 4.75 s major peak in the point plot. The hybrid curve (dotted) appears to provide a qualitative similarity to the point plot curve. The model curve (solid gray) shows two distinct thermal peaks where the first peak is similar to that in the hybrid curve. The hybrid curve displays a low intensity shoulder on the high temperature side of peak 1 at the same pyrolysis time as that of the model curve with a T_{max} of 712 K. The second broad peak in the point plot at approximately 5.75 s appears at a lower GC injection time at 6.5 s after pyrolysis than that for the model and hybrid curves. The hybrid curve provides a more satisfactory description of the point plot than the model curve.

Fig. 8 provides Py–GC–IMS thermal decomposition information for *B. megaterium*. Fig. 8a shows successive 0.5 s GC–IMS dataspaces consisting of the pyrolyzate species of *B. megaterium* spores. The summation value of all the intensities in a GC–IMS dataspace (Fig. 8a) is plotted as a point for GC injection time versus total intensity in Fig. 8b. A cubic spline profile (bold solid curve) was constructed to fit the points in Fig. 8b. The pyrolysis temperature (bold line with a plateau at 7–9 s) over the heating time is shown in Fig. 8b and is the same as that for the other bacilli (Figs. 6b and 7b). The point plot shows two clear thermal events that have a high degree of overlap, and there is no clear peak or shoulder indicating a third thermal event (Fig. 8b). The model curve (gray solid curve) has two major peaks that are resolved, and both peaks have higher T_{max} values than their point plot counterparts. The second peak in the model curve has a similar

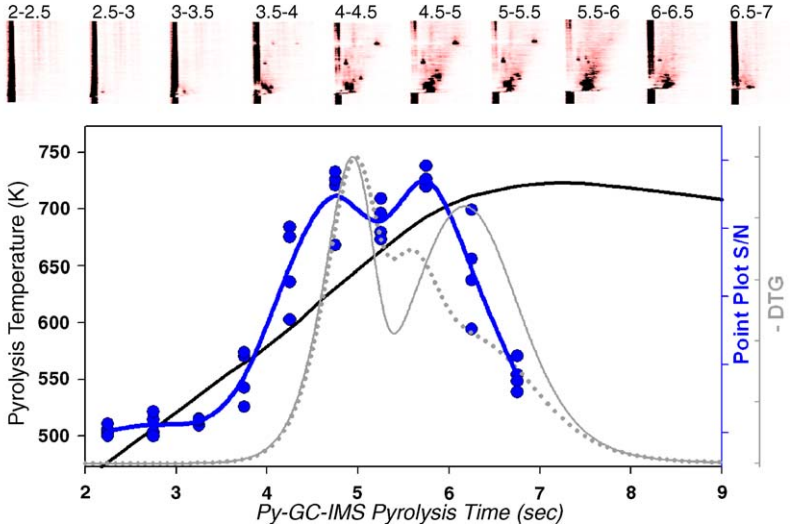

Fig. 8. (a and b) Py–GC–IMS thermal product information for *B. megaterium* spores; see Fig. 6 caption for details.

peak width as that in the point plot, and the T_{max} occurs at a higher temperature (703 K) than that of the point plot at 690 K.

The hybrid curve (dotted) shows two distinct peaks with a low intensity third peak at 6.75 s. The hybrid curve has a high degree of overlap for all three peaks. Both model and hybrid curves display peak 1:2 ratios opposite to that of the point plot. The first peak is smaller than the second peak in the point plot, while the model and hybrid curves show the opposite trend.

3.6. Py–GC–IMS thermal weight loss comparisons of the bacilli

Figs. 6b, 7b, and 8b display two major thermal peaks from the pyrolysis generated point plots that show increasing resolution in the order *B. cereus*, *B. atrophaeus*, and *B. megaterium*. The three bacilli occupy sufficiently different groupings/branches in the taxonomic phylogenetic tree [30,31] based on the V1–V3 region of the 16S rRNA. This differential taxonomic branching structure may partially account for the relative differences in inherent biochemical constituents that can provide an overall pyrolyzate compound distribution. These distributions may be diverse enough to partially account for the different degree of resolution in pyrolyzate generation time and hence resolution of the two main groups of thermal species shown in Figs. 6b, 7b, and 8b.

The model and hybrid −DTG curves of each Bacillus organism display a greater resolution of the first two thermal peaks than that of their respective point plots. It appears that the *B. cereus* and *B. megaterium* model and hybrid curves have higher T_{max} values for the first two peaks compared to the respective peaks in the point plots. For *B. atrophaeus*, the point plot and model −DTG curves have very similar peaks 1 and 2 T_{max} values. The T_{max} for the first peak in the point plots for the three bacilli are represented to a satisfactory degree by both model and hybrid −DTG curves. The second peak in both model and hybrid curves tracks that of the point plot to a satisfactory degree for *B. atrophaeus* (Fig. 6b) and to a lesser extent for *B. cereus*. The second peak in the hybrid curve of *B. megaterium* (Fig. 8b) has a very similar T_{max} to that of the point plot, and the T_{max} of the second peak in the model curve is significantly higher than that of the point plot and hybrid curves.

4. Conclusions

The thermal evolution of biochemical species from highly complex Bacillus spore analytes was investigated by laboratory TGA-MS and an outdoors fielded Py–GC–IMS system. An important goal was to relate laboratory thermo-analytical instrumentation rate of kinetic reaction results to a bioaerosol detector that processes biological species by pyrolysis heating. The current work presents the qualitative biochemical product evolution over time from Bacillus spores. Bacillus species were subjected to kinetic analyses of their thermal decomposition under 200 and 3300 K min^{-1} rates of heating. The fundamental rate of reaction and temperature change equations were used to calculate models of thermal decomposition profiles of Bacillus bacterial spore species. TGA weight loss information was transformed into −DTG profiles which accentuated groups of biochemical compound losses from the solid bacterial analyte in the heating pan. The biochemical compound groups were manifested as distinct thermal peaks in the −DTG curves. This information was qualitatively compared to the thermal processing of the same bacterial spores by the Py–GC–IMS outdoors fielded bioaerosol detector. An overall similarity was observed between the thermal features in the experimental, model, and hybrid −DTG curves for the TGA and Py–GC–IMS experiments.

TGA-MS provided laboratory information in the characterization and interpretation of the heating parameter effects and their inter-relationships with respect to the outdoor-fielded Py–GC–IMS bioaerosol detector for microorganisms. The TGA-MS was also used to modify, optimize, and refine the heating parameter settings on the pyrolysis module in the Py–GC–IMS for bacterial analysis.

The outdoors bioaerosol Py–GC–IMS detection system appears to produce similar thermal product evolution information compared to that of a more sophisticated TGA system.

References

[1] L. Yu, J. Pharm. Sci. 84 (1995) 966–974.
[2] R.B. Cassel, R. Behme, Am. Lab. 36 (2004) 26–29.
[3] G.W. Stowell, R.J. Behme, S.M. Denton, I. Pfeiffer, F.D. Sancilio, L.B. Whittall, R.B. Whittle, J. Pharm. Sci. 91 (2002) 2481–2488.
[4] J.H. Campbell, G.J. Koskinas, N.D. Stout, Fuel 57 (1958) 372–376.
[5] R.L. Braun, A.K. Burnham, Energy Fuels 1 (1987) 153–160.
[6] H.S. Fogler (Ed.), Elements of Chemical Reaction Engineering, Prentice Hall Inc., NJ, 1999, pp. 68–81 (Chapter 3).
[7] A. Tripathi, C.L. Vaughn, W. Maswadeh, H.L.C. Meuzelaar, Thermochim. Acta 388 (2002) 183–197.
[8] R.A. Freitas, S. Martin, R.C. Paula, J.P.A. Feitosa, M.-R. Sierakowski, Thermochim. Acta 409 (2004) 41–47.
[9] P. Miketova, C. Abbas-Hawks, K.J. Voorhees, T.L. Hadfield, J. Anal. Appl. Pyrolysis 67 (2003) 109–122.
[10] J. Cazes, W.J. Irwin (Eds.), Chromatographic Science Series, Analytical Pyrolysis: A Comprehensive Guide, vol. 22, Marcel Dekker Inc., New York, 1982, pp. 381–431 (Chapter 8).
[11] A.P. Snyder, J.P. Dworzanski, A. Tripathi, W.M. Maswadeh, C.H. Wick, Anal. Chem. 76 (2004) 6492–6499.
[12] P. Teixeira, H. Castro, C. Mohacsi-Farkas, R. Kirby, J. Appl. Microbiol. 83 (1997) 219–226.
[13] Cs. Mohacsi-Farkas, J. Farkas, L. Meszaros, O. Reichart, E. Andrassy, J. Thermal Anal. Calorim. 57 (1999) 409–414.
[14] J. Lee, G. Kaletunc, Appl. Environ. Microbiol. 68 (2002) 5379–5386.
[15] J. Lee, G. Kaletunc, J. Appl. Microbiol. 93 (2002) 178–189.
[16] S. Vyazovkin, Anal. Chem. 76 (2004) 3299–3312.
[17] G.W. Gould, Heat-induced injury and inactivation, in: G.W. Gould (Ed.), Mechanisms of Action of Food Preservation Procedures, Elsevier Applied Science, London and New York, 1989, pp. 11–41 (Chapter 2).

[18] B.M. Mackey, C.A. Miles, S.E. Parsons, D.A. Seymour, J. Gen. Microbiol. 137 (1991) 2361–2374.
[19] J. Poznanski, M. Wszelaka-Rylik, W. Zielenkiewicz, Thermochim. Acta 409 (2004) 25–32.
[20] S. Materazzi, R. Curini, Appl. Spectrosc. Rev. 36 (2001) 169–180.
[21] A.P. Snyder, A. Tripathi, J.P. Dworzanski, W.M. Maswadeh, C.H. Wick, Anal. Chim. Acta 536 (2005) 283–293.
[22] A.P. Snyder, W.M. Maswadeh, J.A. Parsons, A. Tripathi, H.L.C. Meuzelaar, J.P. Dworzanski, M.-G. Kim, Field Anal. Chem. Technol. 3 (1996) 315–326.
[23] A.P. Snyder, A. Tripathi, W.M. Maswadeh, J. Ho, M. Spence, Field Anal. Chem. Technol. 5 (2001) 190–204.
[24] G.A. Eiceman, Z. Karpas (Eds.), Ion Mobility Spectrometry, CRC Press, Boca Raton, FL, 1994.
[25] L.K. Nakamura, Intl. J. Syst. Bacteriol. 39 (1989) 295–300.
[26] P.K. Gallagher, R. Blaine, E.L. Charsley, N. Koga, R. Ozao, H. Sato, S. Sauerbrunn, D. Schultze, H. Yoshida, J. Thermal Anal. Calorim. 72 (2003) 1109–1116.
[27] A.P. Snyder, W.M. Maswadeh, A. Tripathi, J.P. Dworzanski, Field Anal. Chem. Technol. 4 (2000) 111–126.
[28] P.A. Demirev, Y.-P. Ho, V. Ryzhov, C. Fenselau, Anal. Chem. 71 (1999) 2732–2738.
[29] F.J. Pineda, J.S. Lin, C. Fenselau, P.A. Demirev, Anal. Chem. 72 (2000) 3739–3744.
[30] F.G. Priest, Systematics and ecology of bacteria, in: A.L. Sonenshein, J.A. Hoch, R. Losick (Eds.), *Bacillus subtilis* and Other Gram-positive Bacteria, American Society for Microbiology, Washington DC, 1993, pp. 3–16 (Chapter 1).
[31] K.S. Blackwood, C.Y. Turenne, D. Harmsen, A.M. Kabani, J. Clin. Microbiol. 42 (2004) 1626–1630.